NeuroImage: Clinical 35 (2022) 103056

Contents lists available at ScienceDirect

NeuroImage: Clinical

journal homepage: www.elsevier.com/locate/ynicl

Multimodal data fusion of cortical-subcortical morphology and functional network connectivity in psychotic spectrum disorder

T.P. DeRamus [a,*], L. Wu [a], S. Qi [b], A. Iraji [a], R. Silva [a], Y. Du [a,c], G. Pearlson [d,e,f], A. Mayer [g], J.R. Bustillo [h], S.F. Stromberg [i], V.D. Calhoun [a,g,j,k,l]

[a] Tri-institutional Center for Translational Research in Neuroimaging and Data Science (TReNDS) - Georgia State University, Georgia Institute of Technology, and Emory University, Atlanta, GA, USA
[b] College of Computer Science and Technology, Nanjing University of Aeronautics and Astronautics, Nanjing, China
[c] School of Computer and Information Technology, Shanxi University, Taiyuan, China
[d] Olin Neuropsychiatry Research Center, Institute of Living at Hartford Hospital, Hartford, CT, USA
[e] Department of Psychiatry, Yale University School of Medicine, New Haven, CT, USA
[f] Department of Neuroscience, Yale University School of Medicine, New Haven, CT, USA
[g] The Mind Research Network, Lovelace Biomedical and Environmental Research Institute, Albuquerque, USA
[h] Department of Psychiatry, University of New Mexico School of Medicine, Albuquerque, NM, USA
[i] Psychiatry and Behavioral Health Clinical Program, Presbyterian Healthcare System, Albuquerque, NM, USA
[j] Department of Electrical and Computer Engineering, Georgia Institute of Technology, Atlanta, USA
[k] Department of Computer Science, Georgia State University, Atlanta, USA
[l] Department of Psychology, Georgia State University, Atlanta, USA

ARTICLE INFO

Keywords:
Multimodal data fusion
Psychotic disorder
Schizophrenia
Bipolar disorder
fMRI
DWI

ABSTRACT

Multiple authors have noted overlapping symptoms and alterations across clinical, anatomical, and functional brain features in schizophrenia (SZ), schizoaffective disorder (SZA), and bipolar disorder (BPI). However, regarding brain features, few studies have approached this line of inquiry using analytical techniques optimally designed to extract the shared features across anatomical and functional information in a simultaneous manner. Univariate studies of anatomical or functional alterations across these disorders can be limited and run the risk of omitting small but potentially crucial overlapping or joint neuroanatomical (e.g., structural images) and functional features (e.g., fMRI-based features) which may serve as informative clinical indicators of across multiple diagnostic categories. To address this limitation, we paired an unsupervised multimodal canonical correlation analysis (mCCA) together with joint independent component analysis (jICA) to identify linked spatial gray matter (GM), resting-state functional network connectivity (FNC), and white matter fractional anisotropy (FA) features across these diagnostic categories. We then calculated associations between the identified linked features and *trans*-diagnostic behavioral measures (MATRICs Consensus Cognitive Battery, MCCB).

Component number 4 of the 13 identified displayed a statistically significant relationship with overall MCCB scores across GM, resting-state FNC, and FA. These linked modalities of component 4 consisted primarily of positive correlations within subcortical structures including the caudate and putamen in the GM maps with overall MCCB, sparse negative correlations within subcortical and cortical connection tracts (e.g., corticospinal tract, superior longitudinal fasciculus) in the FA maps with overall MCCB, and negative relationships with MCCB values and loading parameters with FNC matrices displaying increased FNC in subcortical-cortical regions with auditory, somatomotor, and visual regions.

1. Introduction

An extensive body of literature has reported multiple overlapping clinical symptoms and neuroimaging alterations across schizophrenia (SZ), schizoaffective (SZA), and subgroups of bipolar diagnoses [see (Pearlson, 2015) for a review]. Cognitive impairment across one or more domains is of significant note within individuals on the psychotic spectrum, which has been found across multiple samples of this

* Corresponding author.
E-mail address: tderamus@gsu.edu (T.P. DeRamus).

https://doi.org/10.1016/j.nicl.2022.103056
Received 10 January 2022; Received in revised form 18 April 2022; Accepted 21 May 2022
Available online 23 May 2022

population (Pearlson, 2015; Kern et al., 2004; Burdick et al., 2011; Van Rheenen and Rossell, 2014; Lake and Hurwitz, 2007). As such, many tools for screening cognitive impairment in schizophrenia and schizoaffective diagnosis, such as the MATRICS Consensus Cognitive Battery (MCCB; (Kern et al., 2004), have been applied to bipolar populations (Burdick et al., 2011; Van Rheenen and Rossell, 2014; Lake and Hurwitz, 2007; Yatham et al., 2010; Moller, 2003; Lawrie et al., 2010; Keshavan et al., 2011), and have suggested these three conditions be considered as more of a spectrum of psychotic diagnoses (PSD; (Pearlson, 2015; Kern et al., 2004; Burdick et al., 2011; Van Rheenen and Rossell, 2014). Others have proposed many of these symptoms may be related to genetic, behavioral, and neuroanatomical alterations common to all three conditions (Pearlson, 2015; Lake and Hurwitz, 2007; Potash, 2006; Hanlon et al., 2019). Recent literature even suggests that features overlapping across SZ, SZA, and bipolar (transdiagnostic) capture greater variance in participant functionality than DSM-based classifications (Hanlon et al., 2019). As such, the identification of common, overlapping mechanisms across these disorders is of value and great interest to these populations.

Unfortunately, with regards to neuroimaging, very few studies have investigated this question from a multivariate/multimodal framework, opting instead to study individual diagnoses (e.g., schizophrenia vs control, bipolar disorder vs control), with single neuroimaging modalities (e.g., structural MRI, diffusion MRI, or resting-state connectivity) individually (Sui et al., 2011; Calhoun et al., 2006). The problem with this approach is that individual analyses across modalities significantly reduce power by 1) requiring stringent, multiple comparison corrections for numerous tests across datasets, and 2) failing to account for joint relationships which can be captured via shared within-subject variability across neuroimaging modalities, both of which can drastically reduce an analysis' power to detect (potentially) meaningful effects (Calhoun and Sui, 2016). Further, non-multivariate fusion approaches are not sensitive to linked hidden structures in the data from different modalities (see Fig. 3 in (Yatham et al., 2010). Instead, co-registration (spatial alignment), regularization (with one modality as the reference), or univariate correlation(s) across modalities are deployed. All of which can be more sensitive to noise (Yatham et al., 2010).

One method which can easily be deployed to address these issues is the use of multiset canonical correlation analysis in conjunction with joint independent component analysis (mCCA + jICA; (Sui et al., 2011). In contrast to the univariate approaches described in the previous paragraph, mCCA + jICA has the advantages of: 1) identifying linked hidden structures across multimodal data "features" (e.g., fMRI, diffusion MRI, EEG, ect) using mCCA. 2) Jointly factorize the projected multimodal data into statistically independent modes/components, which are valuable for interpretability and linked by construction. The former (point 1) could be understood as multimodal 'basis alignment' and projection of the data onto that basis rather than co-registration, regularization, or co-registration. First, mCCA is applied across the multimodal features to compute canonical variates. Assuming the correlation(s) among the canonical variates are high, the jICA part of the process will subsequently assume the modalities share the same basis/mixing matrix and consider each modality "linked" based on this shared base assumption (Moller, 2003). From here, jICA then rotates the (multimodal/multifeature) basis by the same amount until overall statistical independence is obtained. The joint (i.e., linked) components learned in the jICA step, the mCCA (modality-specific) and jICA (shared) transformations can then be combined to yield overall modality specific mixing matrices, the columns of which represent 'loadings' for each joint component.

In mCCA + jICA (Fig. 1), we first apply mCCA to obtain the canonical weights (C_i) and the canonical variates (D_i in Fig. 1). The canonical variates (D_i) are a set of multi-modal features (e.g., GM maps, FA maps) which are maximally correlated across participant data (Correa et al., 2010). Next, jICA is deployed on the canonical weights (Fig. 1; $C_s = ZxSs$, $Z = W^{-1}$) to extract shared information across modalities, resulting in a shared mixing matrix (Z) and independent multimodal components (S_i in Fig. 1). The multimodal components are then projected back onto the original data to recover modality-specific loadings ($A_i = D_i xZi$; 12,16). The process of mCCA + jICA can be summarized as $X_k=(D_k xZ)\cdot S_k$, $A_k = D_k xZ$. This approach has been shown to mitigate limitations in both mCCA and jICA (Sui et al., 2011; Sui et al., 2013). Once computed, the mCCA + jICA loadings are then assessed for linear relationships with MCCB scores, as changes in cognition (as measured by MCCB) are typically associated with PSD risk factors (Pearlson, 2015; Kern et al., 2004; Burdick et al., 2011; Van Rheenen and Rossell, 2014).

In this analysis, a multimodal, multivariate mCCA + jICA data fusion analysis is deployed across 193 individuals of multiple diagnostic categories, including SZ, SZA, bipolar I (BPI), plus those without any previous diagnosis (CON). The overall goal of the project is to identify linked (across functional and anatomical sMRI/dMRI information) components related to overall MCCB scores. To do so, each feature from each multimodal component is assessed relative to overall MCCB symptoms scores. Given the relationship between cognition and PSDs, the *trans*-diagnostic utility of each linked (multimodal) feature set is then discussed.

2. Methods

To probe the relationship(s) between MCCB scores and multimodal MRI features, sample participants were recruited from the greater Albuquerque NM area. Participants were scanned at the Mind Research

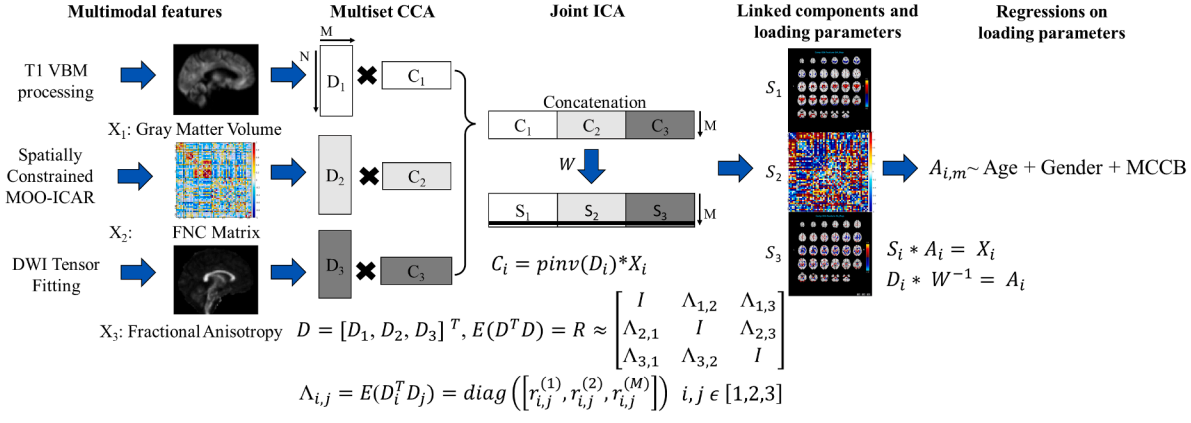

Fig. 1. The whole analysis pipeline starting from initial data (left) to data analysis on loading parameters from mCCA + jICA (right).

Network (MRN) with a Siemens 3 Tesla TIM Trio scanner with a 32-channel head coil. For each participant, three types of images were obtained:

1) High resolution 5-echo multi-echo Magnetization Prepared Rapid Acquisition Gradient Echo (MPRAGE) **T_1-weighted images** [repetition time (TR) = 2530 ms; echo times (TE) = 1.64, 3.5, 5.36, 7.22, 9.08 ms; inversion time (TI) = 1200 ms; flip angle = 7°; number of excitations (NEX) = 1; slice thickness = 1 mm; field of view (FOV) = 256 mm; matrix size = 256 × 256; isotropic voxels = 1 mm], were used as the basis for segmentation to analyze differences in gray matter volume.
2) Resting-state fMRI data included two spin-echo field mapping sequences (TR = 722 msec; TE = 73 msec; flip angle = 90; refocus flip angle = 180; slice thickness = 3 mm; FOV = 247.64 mm; matrix size = 82 × 82; 56 interleaved slices; 3.02 × 3.02 × 3.00 mm^3 voxels) with reversed phase encoding directions (anterior-posterior [AP]; posterior-anterior [PA]) were collected to account for susceptibility distortions in the gradient echo data. Next, a single-band reference (SBRef) image with multiband acceleration factor set to one (i.e., no acceleration) was acquired prior to the time series data to facilitate registration to the T_1-weighted anatomical image. Finally, the **fMRI time series** was acquired using a single-shot, gradient-echo echo planar pulse sequence (TR = 460 msec; TE = 29 msec; flip angle = 44; multiband acceleration factor = 8; NEX = 1; slice thickness = 3 mm; FOV = 247.64 mm; matrix size = 82 × 82) with 56 interleaved 3-mm slices acquired for whole-brain coverage (voxel size: 3.02 × 3.02 × 3.00 mm^3). The data totaled to 650 images of roughly 5-minutes of BOLD information.
3) **High angular resolution dMRI (HARDI)** scans were acquired using a twice-refocused spin-echo sequence with 87 diffusion gradients (29 each at b = 800 s/mm^2, b = 1600 s/mm^2, b = 2400 s/mm^2) and the b = 0 experiment repeated 4 times [72 interleaved slices; TR = 4000 ms; TE = 108 ms; flip angle = 84; refocus flip angle = 157; NEX = 1; voxel resolution = 2.0 × 2.0 × 2.0 mm; FOV = 224 mm; multi-band factor = 3]. The data were collected across 2 runs, with reversed phase encoding direction for each run (AP; PA), totaling 6 min and 36 s. Gradient directions were selected based on guidelines published by (Skare et al., 2000; Jones et al., 2002).

2.1. Participants

Clinical and diffusion MRI (dMRI) results from this sample (Structured Clinical Interview For DSM-IV (SCID-I/SCID-II), 2011) and a similar one (Hanlon et al., 2019) have been published previously with additional measures, but criteria and demographics are repeated below for clarity. All participants provided informed consent and were compensated for participating in accordance with University of New Mexico School of Medicine institutional guidelines. Participants either had no prior history or diagnosis of any psychotic diagnoses [CON, n = 56], or any current diagnosis of SZ [n = 90], SZA [n = 10], or BPI with a history of psychotic features [n = 37]. SZ, SZA, and BPI participants were recruited from local psychiatric centers and, along with CON participants, from advertisements in local newspapers. Diagnoses of SZ, SZA, or BPI were assigned to participants by board-certified psychiatrists based on information from the Structured Clinical Interview for DSM-IV-TR (SCID-II; 19] and clinical record reviews.

Exclusion criteria for all participants consisted of 1) MRI contraindications, 2) intellectual disabilities, 3) history of neurological illness or head injury (loss of consciousness > 30 min), 4) current pregnancy, 5) electroconvulsive therapy, scheduled or performed within the previous month, and 6) current diagnoses of substance use disorders (not including marijuana or nicotine use). In addition, participants were administered urine-based drug screens at both neuropsychological and MRI visits and were excluded if positive results occurred (except for marijuana for PSD). Exclusion specific to CON participants (assessed with SCID-NP for DSM-IV-TR) included 1) history of Axis 1 disorder, 2) history of substance use (except for nicotine), and 3) first-degree relative (s) with a SZ, SZA, or BPI. All participants received the perceived quality-of-life questionnaire for patients with schizophrenia (SQoL; (Boyer et al., 2010)**,** Wechsler Test of Adult Reading (Holdnack, 2001) to estimate premorbid intelligence, and MCCB (2) to determine current cognitive functioning, while participants with SZ, SZA, and BPI were asked to provide additional information regarding history of antipsychotic medication use (Olanzapine equivalence; (Gardner et al., 2010).

We conducted linear regression assessments on two cognitive/affective measures, the SQoL and WTAR metrics, to evaluate interactions between race, ethnic category, self-reported gender, age, years of education, and diagnoses to assess potential interactions in life experience which may affect the analyses of interest. In addition, prior to mCCA + jICA, linear regression assessments were fitted to MCCB overall scores (the *t*-score derived from all 7 MCCB domain scores) to test if the diagnostic group(s) displayed a significant relationship with the MCCB scores while accounting for race, ethnic category, self-reported gender, age, and years of education. The reason for these analyses is twofold. First, to identify variables which may require inclusion in the larger models probing MCCB with mCCA + jICA. Second, to probe the data for the presence of Simpson's (Simpson, 1951) or Lord's (Lord, 1967; Lord, 1969) paradoxes within the data, which have been documented to generate problematic interpretations when not addressed (Kievit et al., 2013; Roberts et al., 2016; Teuscher, 2022).

2.2. Data preprocessing

Each participant's SBRef image and fractional anisotropy (FA) map were co-registered via an affine warp to each participant's anatomical T1 image. Following this transformation, the *antsMultivariateTemplateConstruction2.sh* workflow, where the initializing (bias corrected via *N4BiasFieldcorrection* in *ANTs* v3.0.0.0.dev122-g65096) T1, SBRef, and FA images were affinely warped to MNI space. This workflow produced T1, FA, and EPI templates within a common space used for subsequent registrations.

T1 Images: Each bias-corrected anatomical T1 image (corrected using ANTs' *N4BiasFieldCorrection*) was skullstripped using the *ROBEX* tool (https://www.nitrc.org/projects/robex) and then segmented into gray matter (GM), white matter (WM), and cerebro-spinal fluid (CSF) probability maps using FSL's *FAST*. After which, each image was warped to the study-specific T1 image in MNI space created using *antsMultivariateTemplateConstruction2.sh* using *ANTs*' Greedy Syn Diffeomorphic registration (Avants et al., 2009; Avants et al., 2011). From here, a Jaccobian determinant image was created for each warp utilizing the *CreateJacobianDeterminantImage* function in *ANTs*, and each gray matter map was multiplied by this image to produce a gray matter volume map for mCCA + jICA. Finally, the data were smoothed with a 10 mm full width at half maximum (FWHM) Gaussian kernel and resampled to 2 mm isotropic voxels.

***EPI Images*:** Fieldmap data were collected with phase reversed blips, producing pairs of images with distortion occurring in opposite directions. One volume, acquired with phase encoding in the PA direction, and one volume with phase encoding in the AP direction, were used with the *FSL* (v6.0.3) tool *topup* (Andersson et al., 2003; Smith et al., 2004) to estimate the susceptibility-induced off resonance field. The output fieldmap coefficients were used to correct the distortion in the 4D fMRI volume and SBRef using the FSL tool *applytopup*. The SBRef image collected prior to each time series was co-registered to the native T_1 image for each participant using *FSL*'s boundary-based registration (Greve and Fischl, 2009) procedure. After which, each image was despiked using *AFNI*'s 3dDespike - NEW, then each time series was realigned to the SBRef image using *AFNI*'s *3dvolreg*. Once realigned, the images were warped to the study specific T_1 image in MNI space using the transformations from the co-registration and warp from the T_1 to

study specific template in MNI space derived from the T_1 image pipeline above using *ANTs*' Greedy Syn Diffeomorphic registration (Avants et al., 2009), resampled to 3 mm isotropic voxels, and smoothed to an estimated FWHM of 8 mm using AFNI's *3dBlurToFWHM* tool. Once in the common space, all EPI images were subjected to a spatially constrained form of group information guided ICA (GIG-ICA; (Du and Fan, 2013; Du et al., 2016) called multi-objective optimization with reference (MOO-ICAR) contained within the *Neuromark* pipeline (Du et al., 2020) to compute functional network connectivity (FNC).

***MOO-ICAR*:** Functions from the *GIFT* toolbox (https://trendscenter.org/software/gift/; (Iraji et al., 2020) in Matlab were deployed with in-house workflows distributed across the TReNDS high-performance computing (HPC) environment using a *SLURM* (Yoo et al., 2003) scheduler and resource manager. The pipeline was structured in such a manner that the first 10 images of the 650 non-SBRef time series data were removed to account for T_1 equilibrium effects. The MOO-ICAR approach utilized the components from the *Neuromark* template constructed as part of the Neuromark project (available in GIFT version 4e; (Du et al., 2020) as the references for MOO-ICAR to extract subject-specific independent component maps and their time courses. The Neuromark template includes fifty-three intrinsic connectivity networks (ICNs) and arranged into seven functional domains using visual inspection and atlas labels based on the peak coordinates for each component. These include 2 auditory (AUD), 4 cerebellar (CER), 17 cognitive control (CC), 7 default mode (DM), 5 subcortical (SC), 9 somatomotor (SM), and 9 visual (VIS) components. After obtaining the subject-specific time-courses, the ICN time courses were linearly detrended and filtered between 0.01 and 0.15 Hz prior to FNC calculations. Then, the Pearson correlation coefficient was calculated between time courses of ICNs and r-to-z transformed, resulting in a 53 *x* 53 FNC matrix for each participant. This 53 *x* 53 matrix was then vectorized into a single 1 *x* 1378 vector and entered the mCCA + jICA data fusion pipeline.

Fractional Anisotropy Images: DWI data were collected with phase reversed blips, producing pairs of images with distortion occurring in opposite directions. Volumes with b = 0 (some with phase encoding in the anterior-posterior AP direction and some with phase encoding in the posterior-anterior PA direction) were extracted from the diffusion dataset and used with the *FSL* (v6.0.3) tool *topup* (Andersson et al., 2003; Smith et al., 2004) to estimate the susceptibility-induced off resonance field. DWI volumes were then corrected for eddy current-induced distortions, head movement, and EPI distortions (based on the output from *topup*) using the FSL tool *eddy* (Andersson and Sotiropoulos, 2016). Additional features for advanced motion correction were enabled in eddy to detect and correct motion induced signal dropout (Andersson et al., 2016) and intra-volume (slice-to-volume) movement (Andersson et al., 2017). The latter occurs with interleaved acquisition and produces a "zig-zag" artifact which is corrected by *eddy*, thus allowing all volumes in the dataset to be used for subsequent processing. Fractional anisotropy (FA) maps using the *AFNI* (v.19.1.00) tool *3dDWItoDT* (Taylor and Saad, 2013). The FA maps were then co-registered to each participant's anatomical T_1 image using an affine transformation in *ANTs*, which was then transformed to the T_1 image in MNI space created using the *ANTs* workflow for template generation. The FA maps were then smoothed with a 10 mm FWHM Gaussian kernel with *AFNI*'s *3dmerge*, and then resampled to 2 mm isotropic voxels.

2.3. mCCA + jICA

The complete analysis pipeline is described in Fig. 1. Gray matter volume (GM) maps, FNC matrices, and fractional anisotropy (FA) maps were fed into mCCA + jICA (Sui et al., 2013) for joint multimodal fusion analysis. mCCA was applied to the gray matter volume maps, FNC matrices, and fractional anisotropy maps to extract components, then submitted to ICA using infomax weights as the cost function to maximize independence; producing multi-modal component maps and subject-specific loading parameters. The cost function utilized for the mCCA was the sum of squared correlations and 13 components were resolved from the data. Thirteen components were selected as the number of features resolved by the mCCA + jICA after it was identified that any number of components>13 number (15 were planned the original analysis) were found to be rank-deficient based on the data and could not be resolved.

Once each component was resolved, the *FSL* function *clusterize* was used to identify peaks above a z-threshold of ± 2.5. It is worth noting this threshold is strictly to visualize and label each region within the spatial maps for the gray matter and fractional anisotropy spatial maps and should not be interpreted as cluster-corrected outputs from the analysis. Labels were applied using the Harvard-Oxford cortical and subcortical atlases for GM feature maps, and the JHU White-matter tractography and XTRACT HCP Probabilistic Tract Atlases for the FA feature maps.

2.4. Regressions on loading parameters

For each multimodal feature (GM, FNC, and FA) across the 13 components [3x13], subject-specific loading parameters were regressed onto participant age, self-reported gender, and overall MCCB score as factors of interest. The author's opted to perform 39 (13 components × 3 modalities) individual multiple regressions in lieu of 13 (one for each linked set of components) multivariate multiple regressions due to the discovery that the assumptions for multivariate multiple regression(s) would have been violated across these models. While non-parametric solutions are available for regression-based analyses (e.g. permutation regression, generalized additive models, local regression, etc.), these approaches currently do not have readily deployable packages for multivariate versions of these analyses. While the authors see this as an opportunity to collaboratively develop such analytical tools, such projects are beyond the scope of the manuscript.

The expressed purpose of these models is to identify which linked components (if any) were significantly related to overall MCCB scores. Follow up correlations with sub-scores of the MCCB are performed on components with significant relationships with overall MCCB scores using a Spearman's ρ rank-order correlation due to the ordinal nature of the MCCB scores. However, post-hoc Games-Howell tests (Games and Howell, 1976; Lee and Lee, 2020) *Holm* (Holm, 1979) corrected at the level of each dependent variable) are utilized to examine differences in participant diagnostic status across MCCB scores and any mCCA + jICA factor(s) statistically significant across features for the purpose of interpreting MCCB vs diagnostic status.

3. Results

3.1. Participants

While the number of participants within each group is admittedly skewed, group membership did not differ on age or gender composition. However, noticeable differences were found in years of education between CON participants and individuals with SZ following a *Holm* correction for multiple comparisons (p-value < 0.001). Regressions exploring differences in overall MCCB scores across participant factors met all required assumptions for linear regression. The WTAR model met the assumptions for lack of autocorrelation (p-value = 0.26), outliers, and normal distribution of residuals (p-value = 0.06), but not the assumption of heteroscedasticity (p-value = 0.001; 46) The regression on SQoL model met the assumptions of regression regarding a lack of autocorrelation in the data (p-value = 0.13), and a lack of outliers, but assumptions of heteroscedasticity and non-normality of residuals were violated (p-value = 0.002 & p-value < 0.001, respectively). As such, permutation regression regressions with 10 k permutations were used instead of standard multiple regression for models with WTAR and SQoL as dependent variables.

The regression model informed by gender, participant age, race, ethnic category, education, and diagnostic categories in addition to each factor's interaction with diagnosis found significant influences of participant diagnosis ($F_{(3,163)} = 26.55$, $p < 0.001$), ethnic category ($F_{(3,163)} = 6.2$, $p = 0.002$) and years of education ($F_{(3,163)} = 35.76$, $p < 0.001$). Games-Howell post-hoc analyses computed with the following function (https://gist.github.com/aschleg/ea7942efc6108aedfa9ec98aeb6c2096) on diagnosis identified significantly lower MCCB scores in participants with SZ ($t_{(127.17)} = 8.43$, $p < 0.001$) and BPI ($t_{(63.56)} = 2.879$, $p = 0.03$) relative to CON participants, and lower MCCB in SZ participants compared to BPI participants ($t_{(59.62)} = 3.22$, $p = 0.01$), but no other significant differences. Participants which identified as not Hispanic or Latino displayed higher MCCB scores relative to participants which did identify as Hispanic or Latino ($t_{(177.67)} = 2.8$, $p = 0.02$). The correlation between education and overall MCCB scores was moderate ($\rho = 0.49$, p-value > 0.001), with more years of education associated with higher MCCB scores. Follow-up estimations by the *Simpsons* (https://cran.r-project.org/src/contrib/Archive/Simpsons/) package in *R* did not find any evidence for Simpson's paradoxes in the data based on diagnostic categories relative to ethnicity, gender, or years of education, but one exception was found for individuals on the psychosis spectrum across racial groups. However, the sign inversion of the beta weight for this observation was not significantly different from the beta weight across groups (p-value $= 0.16$). Finally, as an additional analysis, a correlation with overall MCCB domain scores displayed and equivalent olanzapine dose identified a statistically significant negative correlation (ρ = -0.37, p-value > 0.001), where participants with higher olanzapine equivalent medication statuses generally exhibited lower overall MCCB scores than those with lower olanzapine equivalent statuses.

Permutation regressions on raw WTAR scores (adj. $R^2 = 0.315$) did not find main effects for diagnostic groups, but did identify significant influences of education ($F_{(1,163)} = 55.95$, $p < 0.001$) linking more years of education to higher WTAR scores ($\rho = 0.56$, $p < 0.001$) in addition to interactions between diagnostic group and participant's reported racial identities ($F_{(1,163)} = 1.86$, $p = 0.006$), in addition to an interaction between reported racial identity and ethnic identity ($F_{(1,163)} = 0.41$, $p = 0.04$). The nature of these relationships are complicated, as while Caucasian/white and African American/black participants displayed similar WTAR score distributions of SZA > BPI > CON > SZ, American Indian/Native American participants displayed SZA > BPI > SZ > CON distributions, while Asian participants displayed BPI > SZA > CON > SZ distributions, and Native Hawaiian/pacific islander and participants who did not report a racial identity displayed SZ > SZA > BPI > CON distributions. Across reported racial identities, those who did not report as Hispanic or Latino were more likely to have higher raw WTAR scores than those who reported as Hispanic or Latino. However, both interactions should be considered with caution due to the limited range of some of the reported values, and the considerably larger number of Caucasian/white participants relative to other participants. Permutation-based regressions on SQoL did not identify any significant effects of participant diagnosis or any of the other variables analyzed. It should be noted however, the fit for this model was low at adj. $R^2 = 0.086$. Participant demographic information and summaries of findings are presented in Table 1.

3.2. mCCA + jICA & regressions on loading parameters

The results of each regression across all 13 components are summarized in Table 2. Adjusted R^2 values for each model are plotted across all features in Fig. 2 for the purpose of visualizing model fit. While multiple components displayed significant correlations with MCCB Overall scores, only one set of linked components (GM, FA, and rsFNC for component 4) were identified which survived a component-wise *Holm* correction for multiple comparisons.

The images for linked component 4 are summarized below in Table 3 and Fig. 2. The spatial maps for the GM are displayed in Fig. 2a (the first row), the spatial maps for FA results are displayed in Fig. 2b (the second row), and the static FNC (sFNC) matrix configuration most associated with component 4 is displayed Fig. 2c (bottom row), with subcortical-to-cortical connections from the upper left corner of the matrix highlighted (right of figure on row c). Subcortical brain regions, including caudate and putamen, and cerebellum (left areas I-IV and VI, right areas I-IV, VIIIb, and IX) were identified in the GM component. The FA component (Fig. 2b) consisted of multiple white matter regions including the corticospinal tract, forceps major, and left and right superior longitudinal fasciculus. The FNC component (Fig. 2c) consists largely of positive connections between the subcortical regions with auditory, visual, and somatomotor ICNs across the FNC matrix.

3.3. Correlations of linked components with Olanzapine status

The medication status (measured using olanzapine equivalence for each patient group) across SZ, SZA, and BPI did not display any significant Spearman ρ correlations with feature 4 across GM (ρ = -0.14, p-value = 0.113), sFNC (ρ = 0.09, p-value = 0.31), or FA (ρ = 0.06, p-value = 0.50).

3.4. MCCB sub-domain correlations with the linked components

Spearman ρ correlation analyses between loadings of the identified linked components and the MCCB subdomain scores was performed as a follow-up analysis to look for domain-specific relationships between the linked features of component 4 with domain-specific relationships. Results show that GM component is correlated with processing speed (ρ = 0.23, p-value = 0.001) and social cognition (ρ = 0.18, p-value = 0.011), sFNC is correlated with working memory (ρ = 0.22, p-value = 0.002) and social cognition (ρ = -0.24, p-value = 0.<0.001) and FA component is correlated with processing speed (ρ = -0.21, p-value = 0.004), attention/vigilance (ρ = -0.14, p-value = 0.045), verbal learning (ρ = -0.14, p-value = 0.04), and social cognition (ρ = -0.15, p-value = 0.041) sub-domain scores. The analyses and results are summarized in Table 4 below. When post-hoc tests were performed using participant diagnostic

Table 1
Demographic information of participants.

	F/M	Age	Education	WTAR	SQoL	Olanzapine equivalent	MCCB Overall Score
CON	20/36	34.2/32.1	15.4/14.6	38.3/39.7	68.2/65.2	0/0	49.6/47.3
SZ	35/55	32.9/30.9	13.8/12.7	32/33.3	51.5/57.2	12.6/14.4	32/34.2
SZA	4/6	32.8/30.3	13.5/12.8	43.5/31.83	62.4/51.5	21.3/13.6	43.3/34.3
BPD	15/22	34.9/32	14.2/14	38/38	53/55.9	4.7/7.7	40.5/41.4
Average WTAR Scores							
	Black/AA	AI/AN	Asian	NH/PI	White/Cauc	Not Reported	
CON	NA/39.6/NA	43/22/NA	NA/46/NA	NA/NA/NA	39/40/34	40/41/NA	
SZ	NA/32/NA	27/24/NA	NA/32/NA	NA/36/NA	36/30/NA	33/47/NA	
SZA	NA/NA/NA	NA/NA/NA	NA/33/NA	NA/NA/NA	46/34/NA	NA/NA/NA	
BPD	NA/43/NA	31/35/NA	NA/NA/NA	25/NA/NA	34/41/NA	NA/NA/NA	

• AA = African American, AI/AN = American Indian/Native American, BPD = Bipolar disorder, CON = Control, MCCB = MATRICS Consensus Cognitive Battery, NH/PI = Native Hawaiian/Pacific Islander, SZ = Schizophrenia, SZA = Schizoaffective, WTAR = Wechsler Test of Adult Reading
• Note: Average WTAR scores are reported using the format Hispanic or Latino/Not Hispanic or Latino/Not Reported. NA indicates none of the participants responded with this choice.

Table 2
Regressions across components.

Component	Gender			Age			Overall MCCB			Model			
	Beta	ω_p2	*p*-value	Beta	ω_p2	*p*-value	Beta	ω_p2	*p*-value	$F_{(3,189)}$	*p*-value (uncorrected)	*p*-value (Holm)	Adjusted R^2
GM Feature 1	−4.95E-04	−5.10E-03	8.21E-01	−3.45E-04	3.00E-02	4.60E-03*	1.02E-04	2.52E-03	2.24E-01	3.15	2.62E-02*	4.72E-01	3.25E-02
rsFNC Feature 1	2.38E-03	7.84E-04	3.00E-01	−5.22E-05	−4.02E-03	6.79E-01	5.92E-03	−1.29E-04	1.44E-01	1.18	3.20E-01	1.35	2.74E-03
FA Feature 1	1.73E-03	6.82E-04	3.86E-01	−1.47E-04	3.18E-03	1.83E-01	1.21E-04	7.61E-03	1.17E-01	1.74	1.60E-01	1.43	1.15E-02
GM Feature 2	5.79E-02	−4.20E-03	5.90E-01	7.58E-04	−2.74E-03	4.66E-01	5.65E-05	3.29E-04	3.04E-01	0.58	6.32E-01	1.16	−6.67E-03
rsFNC Feature 2	6.31E-04	−4.49E-03	6.77E-01	5.73E-05	−2.04E-03	4.91E-01	1.21E-04	2.00E-02	3.78E-02*	1.71	1.67E-01	1.28	1.09E-02
FA Feature 2	−4.82E-03	4.00E-02	7.32E-04*	−3.42E-04	1.65E-05	9.00E-02	4.04E-05	−2.27E-03	4.54E-01	9.44	7.64E-06*	2.28E-04*	1.17E-01
GM Feature 3	−7.53E-04	−5.11E-03	7.04E-01	−1.86E-04	8.09E-03	8.97E-02	1.84E-04	2.00E-02	1.62E-02*	2.83	3.98E-02*	6.37E-01	2.78E-02
rsFNC Feature 3	8.72E-04	−4.56E-03	6.98E-01	1.28E-05	−5.20E-03	9.18E-01	−1.39E-04	8.30E-03	1.07E-01	0.91	4.35E-01	1.31	−1.35E-03
FA Feature 3	−2.40E-04	−5.17E-03	8.99E-01	−1.56E-04	5.31E-03	1.34E-01	1.36E-04	1.00E-02	6.03E-02	1.87	1.36E-01	1.50	1.34E-02
GM Feature 4	1.36E-02	2.70E-01	2.57E-13*	−4.15E-04	8.00E-02	2.17E-05*	1.78E-04	3.00E-02	8.06E-03*	32.55	2.22E-16*	8.66E-15*	3.30E-01
rsFNC Feature 4	5.09E-03	1.00E-02	1.02E-02*	6.19E-04	1.40E-01	3.92E-08*	−2.17E-04	4.00E-02	4.39E-03*	14.44	1.66E-08*	5.64E-07*	1.74E-01
FA Feature 4	−9.09E-03	1.00E-01	5.50E-06*	4.01E-05	−4.81E-03	7.08E-01	−1.72E-04	2.00E-02	2.19E-02*	9.48	7.28E-06*	2.26E-04*	1.17E-01
GM Feature 5	−6.43E-03	4.00E-02	2.93E-04*	−5.54E-04	1.40E-01	3.14E-08*	2.89E-04	8.00E-02	2.51E-05*	19.55	4.41E-11*	1.59E-09*	2.25E-01
rsFNC Feature 5	3.05E-04	−5.18E-03	8.87E-01	3.05E-04	7.04E-03	1.13E-01	3.05E-04	2.96E-03	2.11E-01	1.32	2.71E-01	1.35E + 00	4.90E-03
FA Feature 5	5.84E-03	5.00E-02	1.00E-03*	−3.92E-05	−4.37E-03	6.84E-01	1.14E-05	−5.06E-03	8.66E-01	3.96	9.07E-03*	1.91E-01	4.42E-02
GM Feature 6	3.00E-03	2.00E-02	4.59E-02*	2.66E-05	−4.57E-03	7.47E-01	3.33E-05	−3.43E-03	5.61E-01	1.48	2.21E-01	1.33	7.46E-03
rsFNC Feature 6	5.81E-03	6.00E-02	8.27E-04*	−1.65E-04	1.00E-02	8.23E-02	−7.13E-05	9.41E-04	2.78E-01	5.83	7.83E-04*	2.11E-02*	7.02E-02
FA Feature 6	−1.60E-03	−4.36E-03	3.24E-01	−4.24E-04	1.00E-01	3.57E-06*	4.52E-05	−2.41E-03	4.65E-01	7.75	6.55E-05*	1.83E-03*	9.54E-02
GM Feature 7	−1.40E-02	2.30E-01	1.59E-14*	−4.78E-04	1.20E-01	6.61E-07*	5.21E-05	−1.82E-03	4.21E-01	29.00	1.81E-15*	6.88E-14*	3.04E-01
rsFNC Feature 7	−3.68E-03	1.00E-02	9.16E-02	−5.80E-06	−5.07E-03	9.61E-01	−2.22E-04	3.00E-02	8.32E-03*	3.40	1.90E-02*	3.61E-01	3.61E-02
FA Feature 7	3.18E-03	1.00E-02	9.52E-02	−9.69E-05	−2.91E-04	3.56E-01	−7.66E-05	5.55E-04	2.94E-01	1.75	1.59E-01	1.54	1.15E-02
GM Feature 8	−9.30E-03	4.00E-02	1.58E-03*	−1.73E-04	9.47E-04	2.79E-01	−3.27E-06	−5.20E-03	9.77E-01	3.59	1.47E-02*	2.93E-01	3.90E-02
rsFNC Feature 8	−5.83E-03	2.00E-02	5.27E-02	2.44E-04	6.62E-03	1.41E-01	8.35E-05	−2.45E-03	4.68E-01	2.46	6.45E-02	9.03E-01	2.22E-02
FA Feature 8	−1.77E-03	−1.93E-03	5.47E-01	2.05E-04	2.18E-03	2.06E-01	−2.03E-04	1.00E-02	7.22E-02	1.77	1.54E-01	1.54	1.19E-02
GM Feature 9	−6.92E-03	8.00E-02	5.90E-06*	−2.46E-04	4.00E-02	3.02E-03*	5.42E-05	−4.82E-04	3.42E-01	9.45	7.59E-06*	2.28E-04*	1.17E-01
rsFNC Feature 9	−5.99E-03	6.00E-02	3.48E-04*	6.14E-06	−5.19E-03	9.46E-01	−2.55E-05	−4.36E-03	6.87E-01	4.58	4.02E-03*	9.25E-02	5.30E-02
FA Feature 9	−6.17E-04	−4.95E-03	6.79E-01	−1.03E-04	1.70E-03	2.10E-01	1.42E-04	3.00E-02	1.35E-02*	2.53	5.85E-02	8.78E-01	2.34E-02
GM Feature 10	2.91E-03	3.00E-02	4.34E-02*	−2.95E-04	6.00E-02	2.42E-04*	2.29E-04	8.00E-02	4.56E-05*	12.26	2.30E-07*	7.36E-06*	1.50E-01
rsFNC Feature 10	3.10E-03	5.85E-03	8.24E-02	1.99E-04	1.00E-02	4.35E-02*	−2.10E-04	4.00E-02	2.33E-03*	5.09	2.06E-03*	4.94E-02*	6.01E-02
FA Feature 10	1.97E-03	7.99E-03	1.72E-01	−1.58E-04	2.00E-02	4.74E-02*	−8.78E-05	7.90E-03	1.13E-01	3.12	2.73E-02*	4.72E-01	3.20E-02
GM Feature 11	−3.35E-03	3.65E-03	3.80E-02*	−5.63E-04	1.70E-01	1.40E-09*	8.21E-05	4.03E-03	1.84E-01	14.48	1.58E-08*	5.53E-07*	1.74E-01
rsFNC Feature 11	−7.68E-04	−2.77E-03	6.92E-01	2.40E-04	2.00E-02	2.60E-02*	−4.93E-05	−2.91E-03	5.08E-01	1.94	1.24E-01	1.49	1.45E-02
FA Feature 11	6.66E-04	−5.20E-03	6.43E-01	2.63E-04	5.00E-02	1.04E-03*	−7.23E-05	3.78E-03	1.90E-01	4.16	6.95E-03*	1.53E-01	4.71E-02
GM Feature 12	8.53E-04	−9.69E-04	6.86E-01	−4.61E-04	7.00E-02	1.02E-04*	4.45E-05	−3.62E-03	5.82E-01	5.58	1.10E-03*	2.85E-02*	6.67E-02
	5.66E-04	−4.99E-03	8.40E-01	−2.75E-05	−4.92E-03	8.59E-01	−1.47E-04	4.46E-03	1.74E-01	0.65	5.82E-01	1.31	−5.44E-03

(*continued on next page*)

Table 2 (*continued*)

Component	Gender			Age			Overall MCCB				Model		
	Beta	ω_p2	*p*-value	Beta	ω_p2	*p*-value	Beta	ω_p2	*p*-value	$F_{(3,189)}$	*p*-value (uncorrected)	*p*-value (Holm)	Adjusted R^2
rsFNC Feature 12													
FA Feature 12	2.39E-03	2.00E-02	1.65E-01	−5.54E-04	1.40E-01	1.87E-08*	3.24E-04	1.10E-01	1.77E-06*	20.45	1.61E-11*	5.96E-10*	2.33E-01
GM Feature 13	−9.31E-03	1.60E-01	6.69E-09*	−6.71E-06	−5.15E-03	9.37E-01	−4.10E-05	−2.66E-03	4.86E-01	12.66	1.40E-07*	4.62E-06*	1.54E-01
rsFNC Feature 13	−2.52E-03	9.54E-03	1.37E-01	1.27E-04	3.76E-03	1.73E-01	−8.19E-05	3.11E-03	2.07E-01	2.06	1.07E-01	1.38	1.63E-02
FA Feature 13	−3.44E-03	3.00E-02	2.93E-02*	2.22E-04	3.00E-02	1.09E-02*	−1.00E-04	9.06E-03	9.80E-02	5.18	1.84E-03*	4.59E-02*	6.13E-02

• FA: Fractional anisotropy, GM: Gray matter, rsFNC: Resting-state functional network connectivity, ωp^2 = partial omega squared of the variable of interest
• * Indicates significance at $p \leq 0.05$

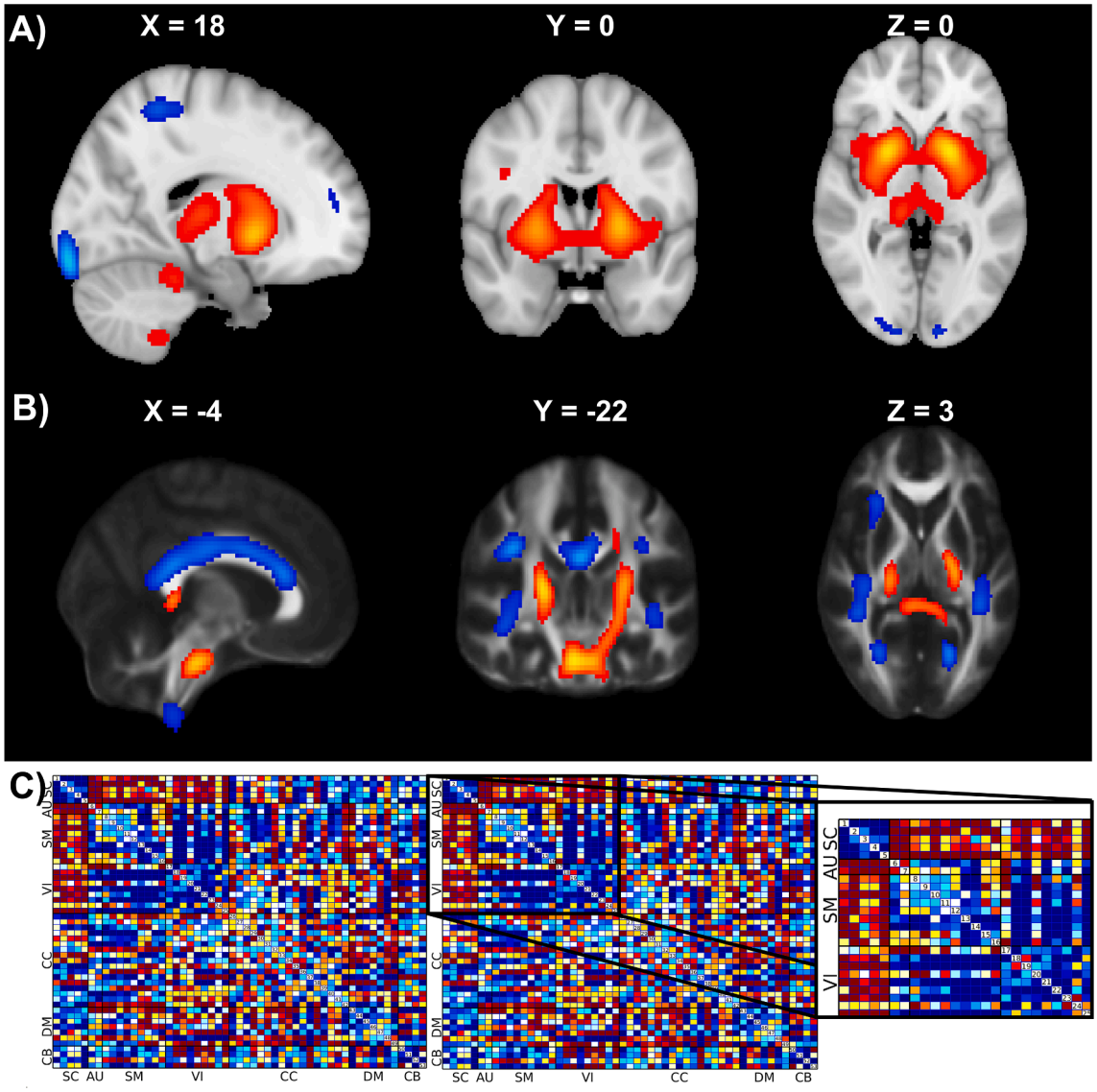

Fig. 2. Spatial maps (thresholded at z= ± 2.5) for A) gray matter and B) fractional anisotropy from component 4. C) Resting-state functional network connectivity matrix configuring the most associations with the linked features of component 4. The image on the far left of C) is the full matrix while the image on the far right of C) is the upper left corner of the FNC matrix highlighting the modularity of subcortical-to-cortical FNC values from the component. Note: The threshold is chosen only for visualization purposes and should not be interpreted as a cluster or voxel-based multiple comparison correction.

Table 3
Cluster Labels for VBM and FA Component 4.

GM Spatial Map						
Voxels	Peak Value	MNI X	MNI Y	MNI Z	Laterality	Label
789	−4.92	20	−94	−14	R	Occipital Pole
614	−4.77	−12	−94	−16	L	Occipital Pole
801	−4.53	−28	−30	54	L	Postcentral Gyrus
947	−4.46	36	−30	52	R	Postcentral Gyrus
74	−3.02	14	54	10	R	Frontal Pole
15	−2.71	40	−26	14	R	Heschl's Gyrus
15	−2.63	−36	−30	12	L	Planum Temporale
5	−2.6	−8	56	10	L	Paracingulate Gyrus
9	2.64	52	−54	−30	R	Cerebellar Crus I
58	3.05	42	2	28	R	Precentral Gyrus
126	3.15	14	−46	−52	R	Cerebellar Area IX
192	3.63	−14	−36	–22	L	Cerebellar Areas I-IV
589	3.67	−26	−62	−26	L	Cerebellar Area VI
341	3.78	16	−38	–22	R	Cerebellar Areas I-IV
7419	9.56	−18	8	2	L/R	Caudate/Putamen
FA Spatial Map						
Voxels	Peak Value	MNI X	MNI Y	MNI Z	Laterality	Label
41,720	−6.08	−18	−66	6	L	Forceps Major
3976	−4.42	−38	−38	6	L	Inferior Longitudinal Fasciculus
2584	−4.36	2	−36	−54	R	Corticospinal Tract
1808	−3.84	36	18	24	R	Frontal Aslant Tract/ Superior Longitudinal Fasciculus
2544	−3.65	20	−34	−28	R	Middle Cerebellar Peduncle
1208	−3.3	−34	−26	30	L	Superior Longitudinal Fasciculus
568	−3.03	−10	−2	14	L	Anterior Thalamic Radiation
128	−2.97	–32	4	24	R	Superior Longitudinal Fasciculus
168	−2.9	26	−62	38	R	–
16	−2.57	−16	−36	−26	L	–
8	2.52	40	−46	−12	R	Inferior Longitudinal Fasciculus
40	2.6	12	38	26	R	–
80	2.65	10	–32	50	R	–
184	2.86	0	−2	−38	L/R	–
144	2.87	−16	48	12	L	Forceps Minor
216	2.91	−14	−14	44	L	–
656	3.16	16	−38	38	R	–
1000	3.21	12	−90	18	R	Forceps Major
1208	3.34	14	6	42	R	Superior Longitudinal Fasciculus
1608	3.56	−12	−92	16	L	Forceps Major
816	3.83	–32	4	36	L	Superior Longitudinal Fasciculus
1568	3.85	−40	−54	−6	L	Inferior Longitudinal Fasciculus
2008	4.15	4	−36	4	R/L	Forceps Major
4520	5.34	22	–22	10	R	Corticospinal Tract
14,480	5.67	4	−24	−26	R	Corticospinal Tract

• FA: Fractional anisotropy, GM: Gray matter, MNI: Montreal Neurological Institute Atlas, VBM: Voxel-based morphometry

status rather than MCCB scores, none of the components or features were significantly different from one another following a *Holm* correction for multiple comparisons. This is despite the finding that MCCB scores only significantly differed between CON and SZ individuals following a *Holm* correction for multiple comparisons ($t_{(127.167)} = 8.43$, *Holm p*-value = <0.001). Results summarizing all pairwise comparisons may be found in Supplementary Table 1 of the manuscript.

Table 4
Correlations across Component 4 with MCCB Subdomains.

MCCB Sub-domain	GM Feature 4	rsFNC Feature 4	FA Feature 4
ρ			
Processing Speed	0.23*	−0.10	−0.21*
Attention/Vigilance	0.05	−0.02	−0.14*
Working Memory	0.09	−0.22*	−0.09
Verbal Learning	0.14	−0.10	−0.14*
Visual Learning	0.11	−0.09	−0.07
Reasoning and Problem Solving	0.04	−0.05	−0.06
Social Cognition	0.18*	−0.24*	−0.15*
p-value			
Processing Speed	1.50E-03*	1.64E-01	4.08E-03*
Attention/Vigilance	4.82E-01	7.79E-01	4.53E-02*
Working Memory	2.00E-01	2.19E-03*	1.90E-01
Verbal Learning	5.35E-02	1.47E-01	4.68E-02*
Visual Learning	1.28E-01	2.06E-01	3.59E-01
Reasoning and Problem Solving	5.89E-01	4.56E-01	4.13E-01
Social Cognition	1.11E-02*	6.60E-04*	4.12E-02*

• FA: Fractional anisotropy, GM: Gray matter, MCCB: MATRICS Consensus Cognitive Battery, rsFNC: Resting-state functional network connectivity.
• * significant at $p < 0.05$

4. Discussion

While previous work has utilized mCCA + jICA to distinguish SZ and BPI from controls (Sui et al., 2011), this study is, to our knowledge, the first case where mCCA + jICA has been leveraged with multimodal data fusion to produce covariance across 3 modalities along the psychotic spectrum continuum, and the first to utilize a GIG-ICA based FNC matrix to link FNC components. The linked components which correlate with overall MCCB scores across control, SZ, SZA, and BPI seem to generate a narrative of subcortical-to-cortical alterations, which is an argument not novel to any of the individual diagnostic categories. For example, previous work (Mamah et al., 2016; Womer et al., 2014) has also noted significant differences in subcortical structures such as the caudate and putamen across SZ and BPI relative to control participants. However, this is potentially confounded by the medication status of the participants, as these have been shown to influence the volume of subcortical structures (Haijma et al., 2013).

The loading coefficients from the sFNC display a pattern of increased FNC between subcortical structures (including the thalamus, caudate, putamen, and subthalamic nucleus) with auditory (superior temporal and insula), visual (including lingual gyrus, occipital pole, and others) and somatomotor regions (including the precentral, postcentral gyri and other regions), but reduced within-network FNC within these same regions. Further, there are multiple studies reporting altered subcortical-to-cortical connectivity in SZ and BPI, but these are typically reported across thalamocortical connections (Sui et al., 2011). Previous work in a large-scale multi-site study noted alterations in similar networks in individuals on the schizophrenia portion of the psychotic spectrum (Skåtun et al., 2017) and it has been argued by multiple research groups that individuals with schizophrenia may display alterations within the striatal-thalamo-cortical loop (Sui et al., 2011; Skåtun et al., 2017; Sui et al., 2015; Sui et al., 2018; Ellison-Wright and Bullmore, 2009; Skudlarski et al., 2013; Heng et al., 2010; Babaeeghazvini et al., 2021). This loop is a key mechanism in inhibitory control, which has been proposed to interplay with working memory (Lustig et al., 2005). This relationship may be reflected in the correlations with working memory scores of the MCCB.

Notable reductions in corticospinal and superior longitudinal white matter tracts have been reported in diffusion specific studies in schizophrenia (Sui et al., 2015; Sui et al., 2018; Zeng et al., 2016), and bipolar disorder (Chang et al., 2018; O'Donoghue et al., 2017; Squarcina et al., 2017). In addition, previous work has, however, found correlations with

symptom scores shared across both clinical groups (Skudlarski et al., 2013). As such, it is possible that these results represent covariance across linked components when multiple participants from the psychotic spectrum are present. However, it was also recently found in a similar study that FA within the corticospinal tract and other regions may be influenced by attention and executive function skills training (which are measured by the MCCB) in individuals with schizophrenia even when no initial reductions in FA are present within these regions (Subramaniam et al., 2018). As such, the patterns could reflect generic changes in training across these domains rather than facets unique to psychotic spectrum disorders.

Previous work by (Sui et al., 2015) noted multi-factorial relationships between caudate volumes, functional amplitude low frequency fluctuations (fALFF) in subcortical structures, and alterations within the superior longitudinal fasciculus specific to individuals with schizophrenia. But the findings presented as part of the current work may highlight a relationship in which alterations within these regions are consistent across the psychotic spectrum. As such, this could highlight a novel mechanism across the psychotic spectrum found using covarying information across linked modalities which would otherwise go unnoticed in univariate analyses. However, additional work with larger and more balanced samples will likely be necessary to establish this relationship.

The observation that the MCCB sub-domain scores vary across the modalities observed in component 4 are interesting and suggest each may influence different roles across the psychotic spectrum. For example, much work implicates subcortical structures like those outlined in the GM components in processing speed and decision making (Meng et al., 2017), which is correlated with MCCB sub-domain scores within this sample.

The social cognition sub-domain results are somewhat more complicated however, as all the features across component 4 correlated with the social cognition MCCB score. There are fair arguments that more than a few of these regions have been involved in the "social brain" to some degree or another, including the cerebellum (Sokolov, 2018), subcortical-to-cortical visual processing streams (Butler et al., 2007), and top-down frontal-visual processing mechanisms such as those mediated by the superior longitudinal fasciculus (Marshall et al., 2015; Braddick et al., 2017). As such, it could be argued that the relationship across all the features specific to social cognition reflect the multifactorial nature of social processing.

4.1. Limitations

The skewness of the groups is a limiting factor of the study, roughly a 62% ratio of CON to SZ participants, 66% ratio of BPI with psychotic features to CON participants, and only 10 SZA participants creating a fair amount of heterogeneity in the data. As such, multivariate multiple regression was not able to be deployed, with the authors opting for a series of single multiple regressions with a Holm correction for multiple comparisons. While this does decrease power regarding test–retest reliability, this is a much more appropriate approach to the analysis given the distribution of the data.

It is worth noting that several of the partial omega squared values and follow-up correlations for age, in addition to pairwise differences, effect sizes are much larger for some age and gender effects compared to overall MCCB scores. As such, it is possible there were significant interactions with these variables not accounted for in the model used for this study. Further, there is also the possibility that these variables could display mediating or moderating effects on the relationship between MCCB scores and the features of interest. Future studies with greater statistical power and more balanced groups should consider modeling and examining this relationship in detail.

As explained previously, alterations in the caudate and putamen are notable, but difficult to interpret considering the history of research noting caudate and putamen volume can be significantly influenced by continuing consumption antipsychotic medications (Haijma et al., 2013). Given this relationship, it may be possible that feature 4 may reflect some degree of medication status that was not fully modeled within the analysis, which future research may wish to explore. Further, the data from which our sample was collected did not differentiate non-psychotic BPI from psychotic BPI, and only included BPI as opposed to BPII participants. As such, the BPI participants in this sample may not reflect the full spectrum of this population.

Further, the finding of no statistically significant differences across diagnostic categories across component 4 across all features raise the argument such alterations may have stronger associations with cognitive decline as measured by MCCB rather than a *trans*-diagnostic feature shared across PSDs. Given that cognitive decline has frequently been found to be the shared feature across PSD [1–4], this difference is difficult to analyze within the current framework.

Declaration of Competing Interest

The authors declare that they have no known competing financial interests or personal relationships that could have appeared to influence the work reported in this paper.

Acknowledgements

General:

The authors would like to thank the participants for their contributions, which made this research possible. Additional acknowledgements should be given to Srinivas Rachakonda for his continued maintenance and development of the GIFT & FIT toolboxes. Finally, the authors would like to acknowledge the contributions of all *R* package developers (particularly *performance* and *permuco*, who have been cited in the references section), and Aaron Schlegel's (https://gist.github.com/aschleg) implementation of the Games-Howell post-hoc test which does not have an official *CRAN* citation.

Funding Sources:

NIHM R01MH118695.
NIHM R01MH123610.
NIMH R01MH101512.
NIGMS P30GM122734.
NSF 2112455.

Appendix A. Supplementary data

Supplementary data to this article can be found online at https://doi.org/10.1016/j.nicl.2022.103056.

References

Andersson, J.L.R., Skare, S., Ashburner, J., 2003 Oct. How to correct susceptibility distortions in spin-echo echo-planar images: application to diffusion tensor imaging. Neuroimage 20 (2), 870–888.

Andersson, J.L.R., Sotiropoulos, S.N., 2016 Jan. An integrated approach to correction for off-resonance effects and subject movement in diffusion MR imaging. Neuroimage 15 (125), 1063–1078.

Andersson, J.L.R., Graham, M.S., Zsoldos, E., Sotiropoulos, S.N., 2016 Nov. Incorporating outlier detection and replacement into a non-parametric framework for movement and distortion correction of diffusion MR images. Neuroimage 1 (141), 556–572.

Andersson, J.L.R., Graham, M.S., Drobnjak, I., Zhang, H., Filippini, N., Bastiani, M., 2017 May. Towards a comprehensive framework for movement and distortion correction of diffusion MR images: Within volume movement. Neuroimage 15 (152), 450–466.

Avants, B.B., Tustison, N., Song, G., 2009. Advanced Normalization Tools (ANTS). Insight J. 1–35.

Avants, B.B., Tustison, N.J., Song, G., Cook, P.A., Klein, A., Gee, J.C., 2011 Feb 1. A reproducible evaluation of ANTs similarity metric performance in brain image registration. Neuroimage 54 (3), 2033–2044.

Babaeeghazvini, P., Rueda-Delgado, L.M., Gooijers, J., Swinnen, S.P., Daffertshofer, A., 2021 Oct. Brain Structural and Functional Connectivity: A Review of Combined Works of Diffusion Magnetic Resonance Imaging and Electro-Encephalography. Front. Hum. Neurosci. 7 (15), 721206.

Boyer, L., Simeoni, M.-C., Loundou, A., D'Amato, T., Reine, G., Lancon, C., et al., 2010 Aug. The development of the S-QoL 18: a shortened quality of life questionnaire for patients with schizophrenia. Schizophr. Res. 121 (1–3), 241–250.
Braddick, O., Atkinson, J., Akshoomoff, N., Newman, E., Curley, L.B., Gonzalez, M.R., et al., 2017 Dec. Individual differences in children's global motion sensitivity correlate with TBSS-based measures of the superior longitudinal fasciculus. Vision Res. 141, 145–156.
Burdick, K.E., Goldberg, T.E., Cornblatt, B.A., Keefe, R.S., Gopin, C.B., Derosse, P., et al., 2011 Jul. The MATRICS consensus cognitive battery in patients with bipolar I disorder. Neuropsychopharmacology 36 (8), 1587–1592.
Butler, P.D., Martinez, A., Foxe, J.J., Kim, D., Zemon, V., Silipo, G., et al., 2007 Feb. Subcortical visual dysfunction in schizophrenia drives secondary cortical impairments. Brain 130 (Pt 2), 417–430.
Calhoun, V.D., Sui, J., 2016 May. Multimodal fusion of brain imaging data: A key to finding the missing link(s) in complex mental illness. Biol. Psychiatry Cogn. Neurosci. Neuroimaging 1 (3), 230–244.
Calhoun, V.D., Adali, T., Giuliani, N.R., Pekar, J.J., Kiehl, K.A., Pearlson, G.D., 2006 Jan. Method for multimodal analysis of independent source differences in schizophrenia: combining gray matter structural and auditory oddball functional data. Hum. Brain Mapp. 27 (1), 47–62.
Chang, M., Womer, F.Y., Edmiston, E.K., Bai, C., Zhou, Q., Jiang, X., et al., 2018 Jan 13. Neurobiological commonalities and distinctions among three major psychiatric diagnostic categories: A structural MRI study. Schizophr. Bull. 44 (1), 65–74.
Correa, N.M., Eichele, T., Adali, T., Li, Y.-O., Calhoun, V.D., 2010 May 1. Multi-set canonical correlation analysis for the fusion of concurrent single trial ERP and functional MRI. Neuroimage 50 (4), 1438–1445.
Du, Y., Fan, Y., 2013 Apr. Group information guided ICA for fMRI data analysis. Neuroimage 1 (69), 157–197.
Du, Y., Allen, E.A., He, H., Sui, J., Wu, L., Calhoun, V.D., 2016 Mar. Artifact removal in the context of group ICA: A comparison of single-subject and group approaches. Hum. Brain Mapp. 37 (3), 1005–1025.
Du, Y., Fu, Z., Sui, J., Gao, S., Xing, Y., Lin, D., et al., 2020 Aug. NeuroMark: An automated and adaptive ICA based pipeline to identify reproducible fMRI markers of brain disorders. Neuroimage Clin. 11 (28), 102375.
Ellison-Wright, I., Bullmore, E., 2009 Mar. Meta-analysis of diffusion tensor imaging studies in schizophrenia. Schizophr. Res. 108 (1–3), 3–10.
Games, P.A., Howell, J.F., 1976. Pairwise Multiple Comparison Procedures with Unequal N's and/or Variances: A Monte Carlo Study. J. Educ. Stat. 1 (2), 113.
Gardner, D.M., Murphy, A.L., O'Donnell, H., Centorrino, F., Baldessarini, R.J., 2010 Jun. International consensus study of antipsychotic dosing. Am. J. Psychiatry 167 (6), 686–693.
Greve, D.N., Fischl, B., 2009 Oct 15. Accurate and robust brain image alignment using boundary-based registration. Neuroimage 48 (1), 63–72.
Haijma, S.V., Van Haren, N., Cahn, W., Koolschijn, P.C.M.P., Hulshoff Pol, H.E., Kahn, R. S., 2013 Sep. Brain volumes in schizophrenia: a meta-analysis in over 18 000 subjects. Schizophr. Bull. 39 (5), 1129–1138.
Hanlon, F.M., Yeo, R.A., Shaff, N.A., Wertz, C.J., Dodd, A.B., Bustillo, J.R., et al., 2019 Jan. A symptom-based continuum of psychosis explains cognitive and real-world functional deficits better than traditional diagnoses. Schizophr. Res. 31 (208), 344–352.
Heng, S., Song, A.W., Sim, K., 2010 May. White matter abnormalities in bipolar disorder: insights from diffusion tensor imaging studies. J. Neural Transm. 117 (5), 639–654.
Holdnack, H.A., 2001. Wechsler test of adult reading: WTAR. The Psychological Corporation, San Antonio, TX.
Holm, S., 1979. A simple sequentially rejective multiple test procedure. Scand. J. Stat. 65–70.
Iraji, A., Faghiri, A., Lewis, N., Fu, Z., Rachakonda, S., Calhoun, V.D., 2020 Aug 12. Tools of the trade: Estimating time-varying connectivity patterns from fMRI data. Soc. Cogn. Affect Neurosci.
Jones, D.K., Griffin, L.D., Alexander, D.C., Catani, M., Horsfield, M.A., Howard, R., et al., 2002 Oct. Spatial normalization and averaging of diffusion tensor MRI data sets. Neuroimage 17 (2), 592–617.
Kern, R.S., Green, M.F., Nuechterlein, K.H., Deng, B.-H., 2004 Dec 15. NIMH-MATRICS survey on assessment of neurocognition in schizophrenia. Schizophr. Res. 72 (1), 11–19.
Keshavan, M.S., Morris, D.W., Sweeney, J.A., Pearlson, G., Thaker, G., Seidman, L.J., et al., 2011 Dec. A dimensional approach to the psychosis spectrum between bipolar disorder and schizophrenia: the Schizo-Bipolar Scale. Schizophr. Res. 133 (1–3), 250–254.
Kievit, R.A., Frankenhuis, W.E., Waldorp, L.J., Borsboom, D., 2013 Aug. Simpson's paradox in psychological science: a practical guide. Front. Psychol. 12 (4), 513.
Lake, C.R., Hurwitz, N., 2007 Jul. Schizoaffective disorder merges schizophrenia and bipolar disorders as one disease–there is no schizoaffective disorder. Curr. Opin. Psychiatry 20 (4), 365–379.
Lawrie, S.M., Hall, J., McIntosh, A.M., Owens, D.G.C., Johnstone, E.C., 2010 Dec. The "continuum of psychosis": scientifically unproven and clinically impractical. Br. J. Psychiatry 197 (6), 423–425.
Lee, S., Lee, D.K., 2020 Dec. What is the proper way to apply the multiple comparison test? Korean J. Anesthesiol. 73 (6), 572.
Lord, F.M., 1967 Nov. A paradox in the interpretation of group comparisons. Psychol. Bull. 68 (5), 304–305.
Lord, F.M., 1969. Statistical adjustments when comparing preexisting groups. Psychol. Bull. 72 (5), 336–337.
Lustig, C., Matell, M.S., Meck, W.H., 2005 May. Not "just" a coincidence: frontal-striatal interactions in working memory and interval timing. Memory 13 (3–4), 441–448.
Mamah, D., Alpert, K.I., Barch, D.M., Csernansky, J.G., Wang, L., 2016 Feb. Subcortical neuromorphometry in schizophrenia spectrum and bipolar disorders. Neuroimage Clin. 23 (11), 276–286.
Marshall, T.R., Bergmann, T.O., Jensen, O., 2015 Oct 6. Frontoparietal Structural Connectivity Mediates the Top-Down Control of Neuronal Synchronization Associated with Selective Attention. PLoS Biol. 13 (10), e1002272.
Meng, X., Jiang, R., Lin, D., Bustillo, J., Jones, T., Chen, J., et al., 2017 Jan 15. Predicting individualized clinical measures by a generalized prediction framework and multimodal fusion of MRI data. Neuroimage 145 (Pt B), 218–229.
Moller, H.-J., 2003. Bipolar disorder and schizophrenia: distinct illnesses or a continuum? J. Clin. Psychiatry 64, 23–27.
O'Donoghue, S., Holleran, L., Cannon, D.M., McDonald, C., 2017 Feb. Anatomical dysconnectivity in bipolar disorder compared with schizophrenia: A selective review of structural network analyses using diffusion MRI. J. Affect. Disord. 209, 217–228.
Pearlson, G.D., 2015 Jan. Etiologic, phenomenologic, and endophenotypic overlap of schizophrenia and bipolar disorder. Annu. Rev. Clin. Psychol. 12 (11), 251–281.
Potash, J.B., 2006 Apr. Carving chaos: genetics and the classification of mood and psychotic syndromes. Harv. Rev. Psychiatry 14 (2), 47–63.
Roberts, R.P., Hach, S., Tippett, L.J., Addis, D.R., 2016 Jul. The Simpson's paradox and fMRI: Similarities and differences between functional connectivity measures derived from within-subject and across-subject correlations. Neuroimage 15 (135), 1–15.
Simpson, E.H., 1951 Jul. The interpretation of interaction in contingency tables. J. Roy. Stat. Soc.: Ser. B (Methodol.) 13 (2), 238–241.
Skare, S., Hedehus, M., Moseley, M.E., Li, T.Q., 2000 Dec. Condition number as a measure of noise performance of diffusion tensor data acquisition schemes with MRI. J. Magn. Reson. 147 (2), 340–352.
Skåtun, K.C., Kaufmann, T., Doan, N.T., Alnæs, D., Córdova-Palomera, A., Jönsson, E.G., et al., 2017 Jul 1. Consistent functional connectivity alterations in schizophrenia spectrum disorder: A multisite study. Schizophr. Bull. 43 (4), 914–924.
Skudlarski, P., Schretlen, D.J., Thaker, G.K., Stevens, M.C., Keshavan, M.S., Sweeney, J. A., et al., 2013 Aug. Diffusion tensor imaging white matter endophenotypes in patients with schizophrenia or psychotic bipolar disorder and their relatives. Am. J. Psychiatry 170 (8), 886–898.
Smith, S.M., Jenkinson, M., Woolrich, M.W., Beckmann, C.F., Behrens, T.E.J., Johansen-Berg, H., et al., 2004. Advances in functional and structural MR image analysis and implementation as FSL. Neuroimage 23 (Suppl 1), S208–S219.
Sokolov, A.A., 2018 Jun. The cerebellum in social cognition. Front. Cell. Neurosci. 5, 12.
Squarcina, L., Bellani, M., Rossetti, M.G., Perlini, C., Delvecchio, G., Dusi, N., et al., 2017 Jun 28. Similar white matter changes in schizophrenia and bipolar disorder: A tract-based spatial statistics study. PLoS ONE 12 (6), e0178089.
Structured Clinical Interview For DSM-IV (SCID-I/SCID-II), 2011. SpringerReference. Berlin/Heidelberg: Springer-Verlag.
Subramaniam, K., Gill, J., Fisher, M., Mukherjee, P., Nagarajan, S., Vinogradov, S., 2018. White matter microstructure predicts cognitive training-induced improvements in attention and executive functioning in schizophrenia. Schizophr. Res. 193, 276–283.
Sui, J., Pearlson, G., Caprihan, A., Adali, T., Kiehl, K.A., Liu, J., et al., 2011 Aug 1. Discriminating schizophrenia and bipolar disorder by fusing fMRI and DTI in a multimodal CCA+ joint ICA model. Neuroimage 57 (3), 839–855.
Sui, J., He, H., Pearlson, G.D., Adali, T., Kiehl, K.A., Yu, Q., et al., 2013 Feb. Three-way (N-way) fusion of brain imaging data based on mCCA+jICA and its application to discriminating schizophrenia. Neuroimage 1 (66), 119–132.
Sui, J., Pearlson, G.D., Du, Y., Yu, Q., Jones, T.R., Chen, J., et al., 2015 Dec 1. In search of multimodal neuroimaging biomarkers of cognitive deficits in schizophrenia. Biol. Psychiatry 78 (11), 794–804.
Sui, J., Qi, S., van Erp, T.G.M., Bustillo, J., Jiang, R., Lin, D., et al., 2018 Aug 2. Multimodal neuromarkers in schizophrenia via cognition-guided MRI fusion. Nat. Commun. 9 (1), 3028.
Taylor, P.A., Saad, Z.S., 2013. FATCAT: (an efficient) Functional and Tractographic Connectivity Analysis Toolbox. Brain Connect. 3 (5), 523–535.
Teuscher, F., 2022 Feb 24. The quantification of Simpson's paradox and other contributions to contingency table theory. PLoS ONE 17 (2), e0262502.
Van Rheenen, T.E., Rossell, S.L., 2014 May. An empirical evaluation of the MATRICS Consensus Cognitive Battery in bipolar disorder. Bipolar Disord. 16 (3), 318–325.
Womer, F.Y., Wang, L., Alpert, K.I., Smith, M.J., Csernansky, J.G., Barch, D.M., et al., 2014 Aug 30. Basal ganglia and thalamic morphology in schizophrenia and bipolar disorder. Psychiatry Res. 223 (2), 75–83.
Yatham, L.N., Torres, I.J., Malhi, G.S., Frangou, S., Glahn, D.C., Bearden, C.E., et al., 2010 Jun. The International Society for Bipolar Disorders-Battery for Assessment of Neurocognition (ISBD-BANC). Bipolar Disord. 12 (4), 351–363.
Yoo, A.B., Jette, M.A., Grondona, M., 2003. SLURM: simple linux utility for resource management. In: Feitelson, D., Rudolph, L., Schwiegelshohn, U. (Eds.), Job scheduling strategies for parallel processing. Berlin, Heidelberg, Springer, Berlin Heidelberg, pp. 44–60.
Zeng, B., Ardekani, B.A., Tang, Y., Zhang, T., Zhao, S., Cui, H., et al., 2016 Apr. Abnormal white matter microstructure in drug-naive first episode schizophrenia patients before and after eight weeks of antipsychotic treatment. Schizophr. Res. 172 (1–3), 1–8.

Further reading

Frossard, J., Renaud, O., 2021. Permutation tests for regression, ANOVA, and comparison of signals: thepermuco package. J. Stat. Softw. 99 (15).
Lüdecke, D., Ben-Shachar, M., Patil, I., Waggoner, P., Makowski, D., 2021 Apr 21. performance: An R Package for Assessment, Comparison and Testing of Statistical Models. JOSS. 6 (60), 3139.
R Core team. R Core Team. R: A Language and Environment for Statistical Computing R Foundation for Statistical Computing , Vienna, Austria ISBN 3-900051-07-0, URL https://nam11.safelinks.protection.outlook.com/?url=http%3A%2F%2Fwwwr-project.org%2F&data=05%7C01%7Ce.mishael%40elsevier.com%7C23dab63e00e84bdbd49608da488018f1%7C9274ee3f94254109a27f9fb15c10675d%7C0%7C0%7C637902012256085552%7CUnknown%7CTWFpbGZsb3d8eyJWIjoiMC4wLjAwMDAiLCJQIjoiV2luMzIiLCJBTiI6Ik1haWwiLCJXVCI6Mn0%3D%7C3000%7C%7C%7C&sdata=dFOoVSIPJukFGbcftbS6xxfUTGK8vkJsARQ9qNK8ACs%3D&reserved=0. 2015;55:275–86.